

Supplementary materials for

Spatiotemporal variation in upper crustal seismic anisotropy and V_P/V_S ratio in Groningen gas field, Netherlands: Insights from shear wave splitting

Jaewoo Kim¹ and YoungHee Kim^{1*}

¹*School of Earth and Environmental Sciences, Seoul National University, Seoul 08826, Republic of Korea.*

*Corresponding Author: YoungHee Kim, Tel.: +82-2-880-6735, email:
younghkim@snu.ac.kr

Email Addresses: giox123@snu.ac.kr (J. Kim), younghkim@snu.ac.kr (Y. Kim)

Contents of this file

Tables S1 to S2

Figures S1 to S14

References of the Supporting Information

Introduction

This supporting information contains two tables and 14 figures that support the main article. Tables S1 and S2 show parameters used in the cluster analysis (Teanby et al., 2004) and quadtree gridding provided in TESSA (Johnson et al., 2011), respectively. Figure S1 displays an example of summary plot of the analysis with the manual method. Figure S2 presents an example of the Eigenvalue method for the same event-station pair used in Figure S1. Figure S3 illustrates an example of the cluster analysis method for the same event-station pair used in Figures S1 and S2. Figure S4 shows comparison of results from three different SWS methods, and Figure S5 shows an example of null splitting measurements obtained from the manual method and Eigenvalue method. Figure S6 shows checkerboard test results for δt inversion. Figure S7 shows temporal variation of V_p / V_s for the data acquired from geophones and accelerometers. Figure S8 shows spatial averaged φ with six weighting schemes. Figure S9 displays temporal variation of δtn for the entire data set. Figures S10 and S11 are enlarged versions of northern and southern regions of Groningen in Figure 10a and b, respectively. Streamline map of Groningen with spatial averaged φ is plotted in Figure S12. Figure S13 illustrates spatio-temporal variation of φ from 2014 to 2020 in Groningen. Figure S14 shows modified Wadati diagrams for computing V_p / V_s in different sectors.

Table S1. Parameters used in Cluster Analysis method (Teanby et al., 2004).

Parameter	Value
Minimum window-start point (s)	-0.1
Step for window-start points (s)	0.02
Minimum window-end point (s)	0.1
Maximum S-P (s)	1.5
Signal window for period determination (s)	0.5
Minimum S-wave period (s)	0.1
Maximum S-wave period (s)	2.0
Period factor	3.0
Maximum number of clusters	10
Minimum number of points per cluster	3
Linkage Criterion	‘ward’

Table S2. Parameters used in quadtree gridding provided in TESSA (Johnson et al., 2011).

Parameter	Value
West longitude (°)	6.5
East longitude (°)	7.1
North longitude (°)	53.0
South longitude (°)	53.5
<i>maxnumber</i>	20
<i>minnumber</i>	3
<i>minsize</i> (m)	1000
Node spacing (m)	250

2019 – 10 – 20T03 : 36 : 42.390; NL. G684
 Baz: 84.4 N°E, Aoi: 18.9°, Epicentral: 1.0km, M_L : 0.9
 φ : 172.3 N°E, δt : 10.0 ms, P: 114.8 N°E, Grade: A, Filter: 1.0 | 20.0 Hz

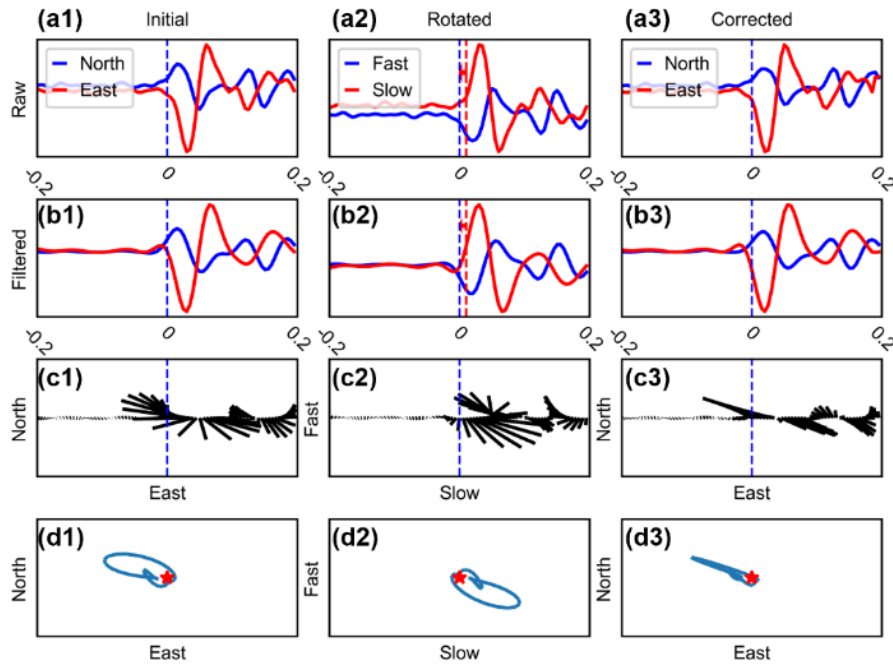


Figure S1. A summary plot obtained from the manual method for one event as an example.

The figure displays raw waveforms (a1-3), bandpass-filtered waveforms (b1-3), polarigrams (c1-3), and particle motions (d1-3). (a1-d1) show a sequence of calculations using the NS- and EW-component waveforms. Similarly, (a2-d2) show results for Fast-Slow (F-S) component waveforms, and (a3-d3) for the corrected NS- and EW-component waveforms. ‘Baz’, ‘Epicentral’, and ‘Aoi’ represent the back azimuth, epicentral distance, and incidence angle of the event-station pair, respectively. ‘P’ indicates expected initial polarization angle of the S wave.

2019 – 10 – 20T03 : 36 : 42.390; NL. G684
 Baz: 84.4 N°E, Aoi: 18.9°, Epicentral: 1.0km, M_L : 0.9
 φ : 2.3 ± 1.4 N°E, δt : 15.0 ± 0.19 ms, P: 112.8 N°E, Grade: A, Filter: 1.0 | 20.0 Hz

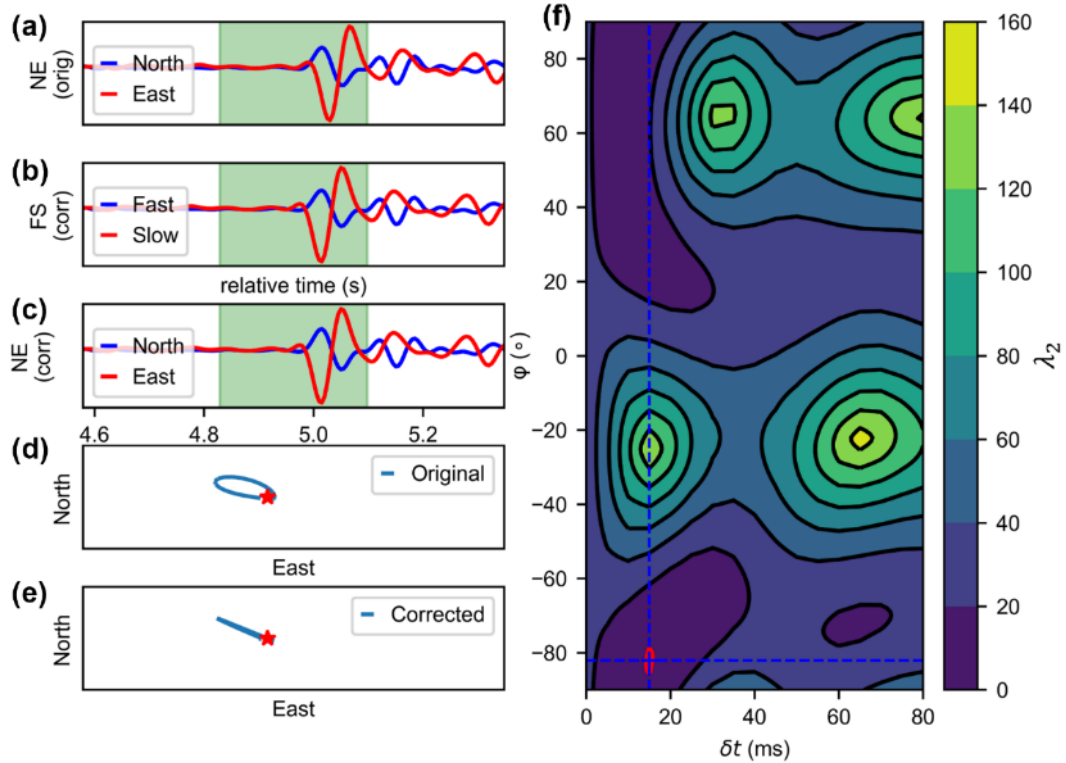


Figure S2. An example showing how the Eigenvalue method works for the same event-station pair used in the manual method (Figure S1). (a-c) present NS and EW component (denoted as NE), rotated F-S component, and corrected waveforms respectively. (d) Particle motion before the shear wave splitting correction. (e) Particle motion after the correction. (f) Contour plot of the second eigenvalue (λ_2). The red contour indicates 95% confidence level.

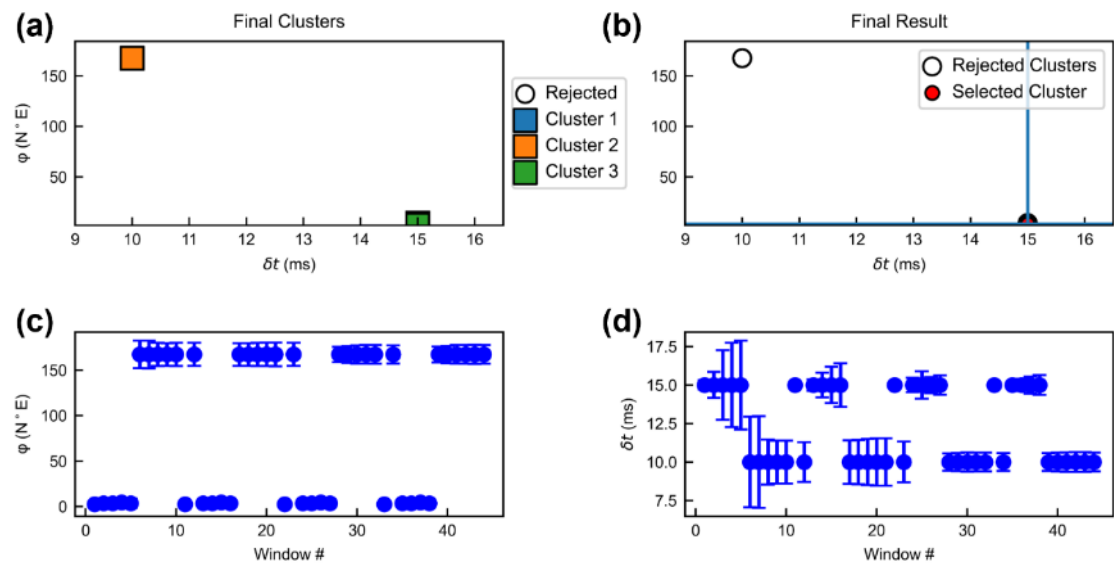


Figure S3. A summary plot obtained from the cluster analysis method using the same event-station pair as a comparison to two other methods (Figures S1 and S2). Panel (a) shows δt and φ for each cluster and rejected one, and panel (b) shows selected and rejected clusters as well as window selection. (c) φ values and their corresponding error bars for different windows. (d) δt values and their error bars for different windows.

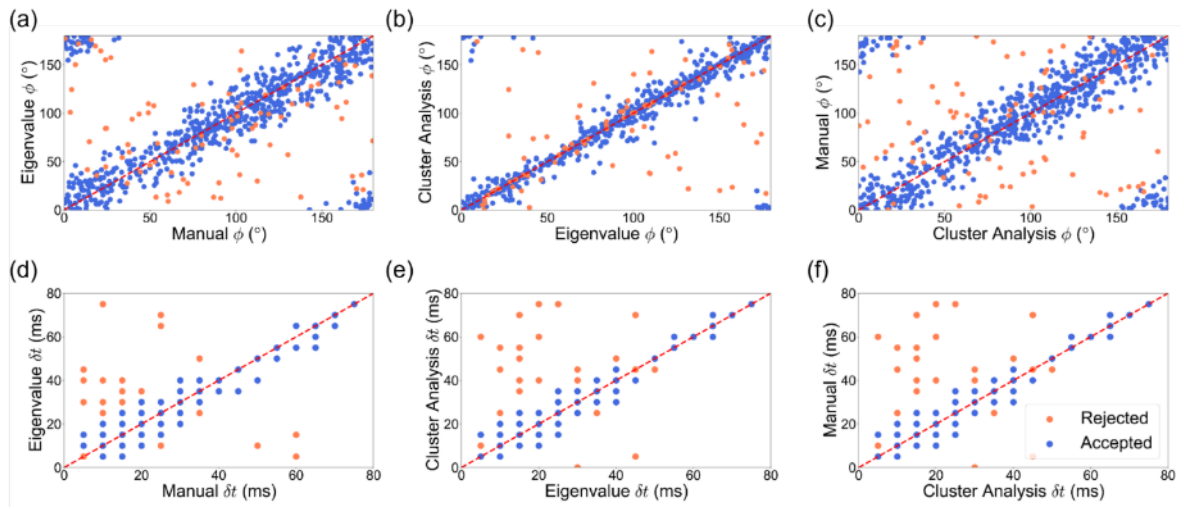


Figure S4. Plots showing the comparison of results obtained from three different SWS methods. Accepted and rejected parameter values are colored in blue and orange, respectively. (a-c) ϕ values obtained from all three methods, (d-f) δt values obtained from all three methods. (a, d) Comparison of manual and eigenvalue method, (b, e) eigenvalue and cluster analysis method, and (c, f) cluster analysis and manual method.

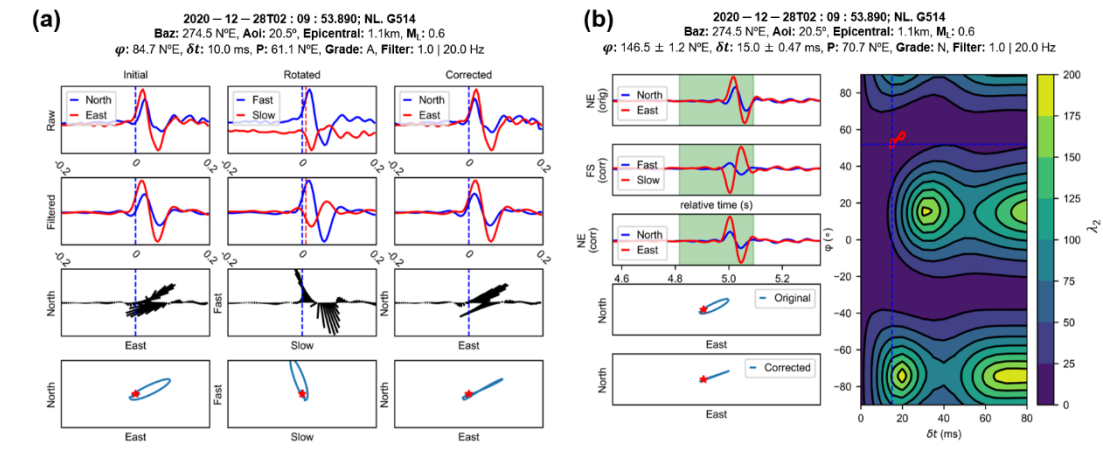


Figure S5. Examples showing null splitting measurements for two different methods. (a) A summary plot for the manual method. (b) A summary plot for the Eigenvalue method. See captions of Figures S1 and S2 for details.

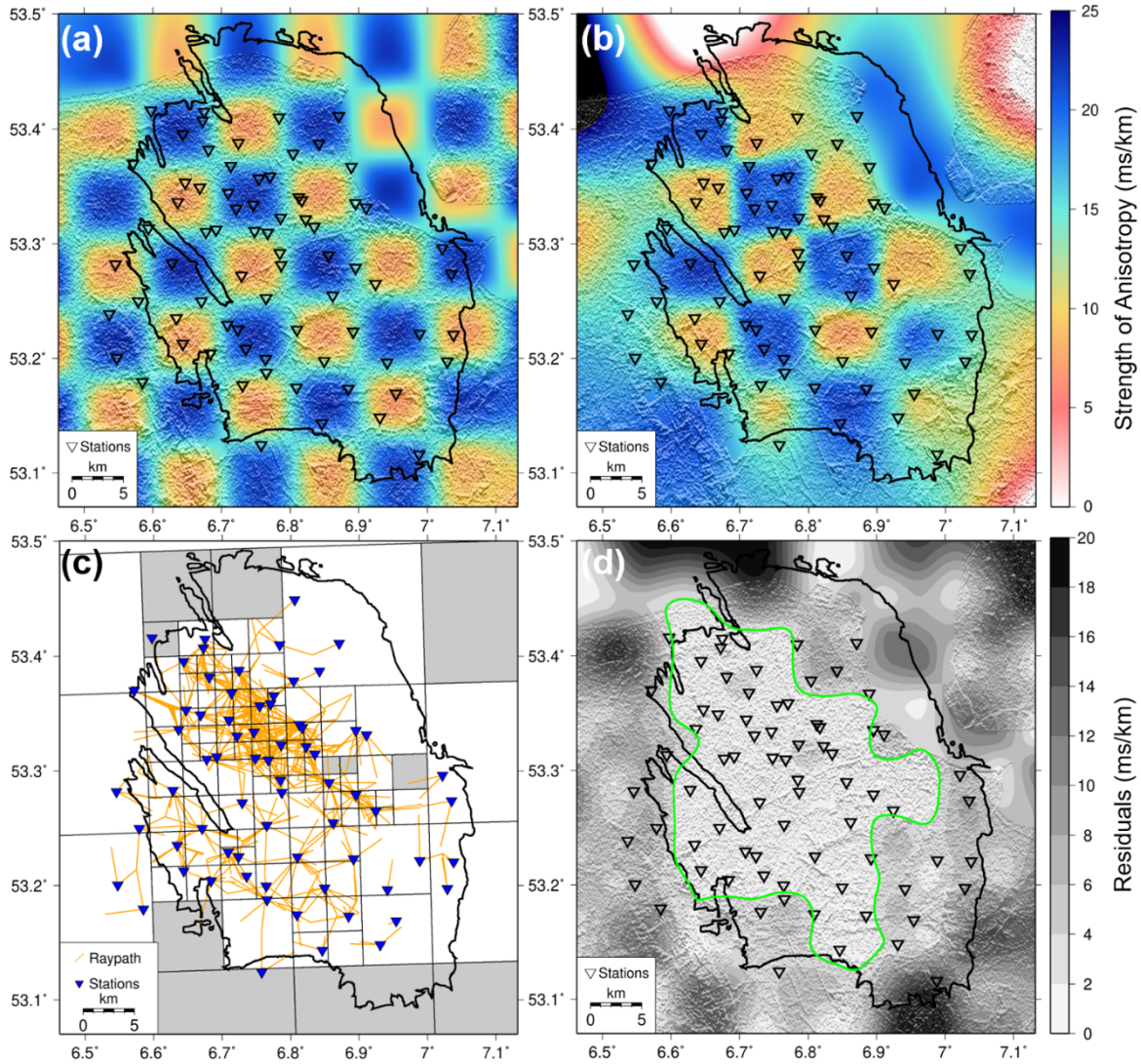


Figure S6. Checkerboard test results for the tomographic inversion of δt . (a) Input checkerboard pattern for the synthetic data. (b) Recovered pattern after the inversion. (c) Map showing grid cells used in the inversion, stations (inverted blue triangles), and ray paths (orange lines). The cells covered with more than three ray paths are used in the inversion, and the cells covered with lesser rays (cells colored in gray) are excluded in the inversion. (d) Residual plot showing the resolution of the model recovered. A green solid line represents residual contour of $2 \text{ ms}/\text{km}$.

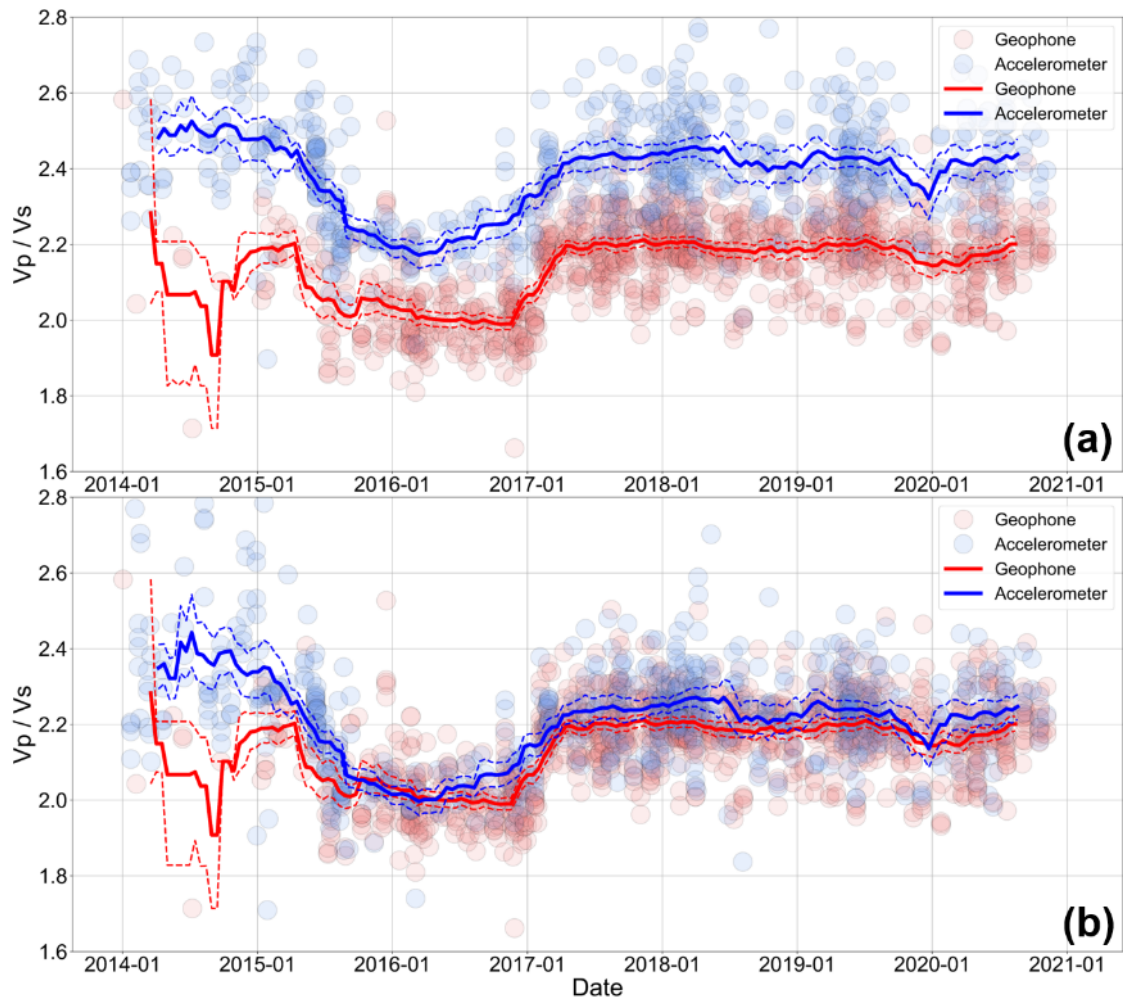


Figure S7. Temporal distribution of V_p/V_s ratio for the data recorded from the geophones at 200 m depth (light pink circles) and surface accelerometers (light blue circles). (a) V_p/V_s ratio obtained before correction. (b) V_p/V_s ratio obtained after correction. Colored solid lines display V_p/V_s values that are averaged with 150-day moving window with 15-day step, and dashed lines show their 95% confidence intervals.

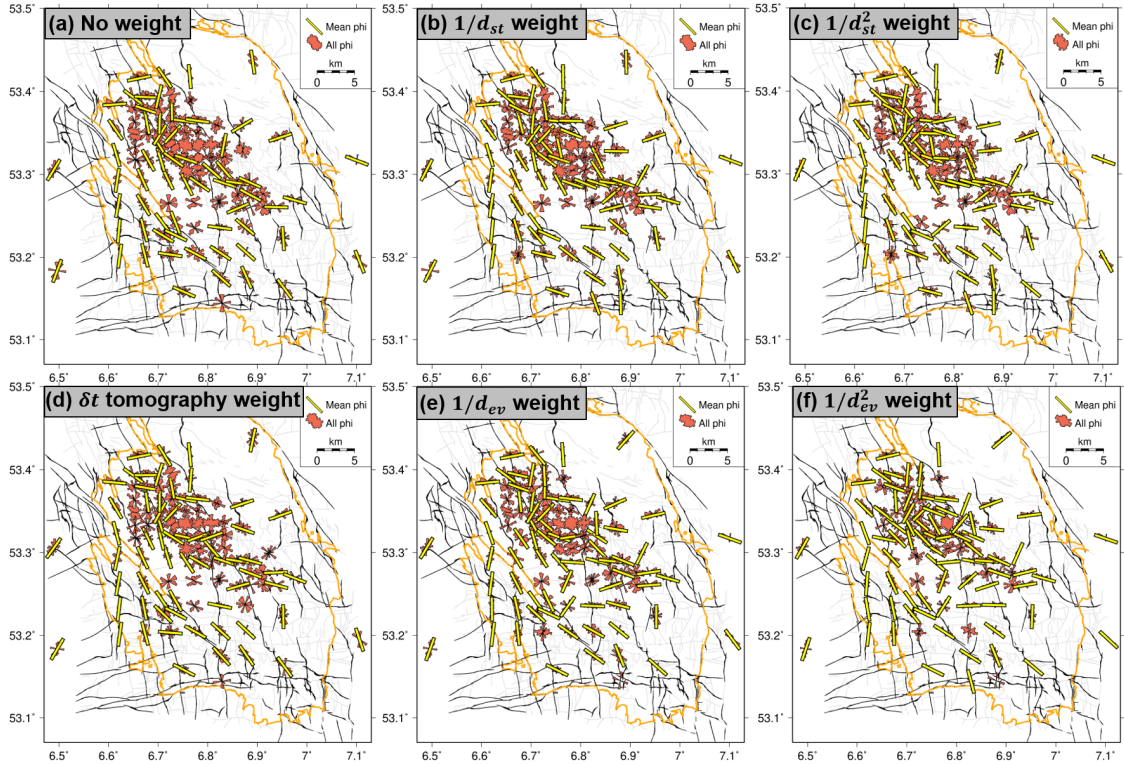


Figure S8. Spatial averages of φ with different weighting schemes. Normalized polar histogram of φ in each grid box is shown with red. Yellow bar illustrates the mean direction of φ . The mean direction is excluded from plotting if standard deviation of φ in the grid box exceeds 25° . The weighting scheme exploited in this study is as follows: (a) no weighting scheme, (b) weighting inversely proportional to the distance from the node to the station, (c) weighting inversely proportional to the square of the distance from the node to the station, (d) weighting from the 2-D δt tomography results, (e) weighting inversely proportional to the distance from the node to epicenter, and (f) weighting inversely proportional to the square of the distance from the node to epicenter.

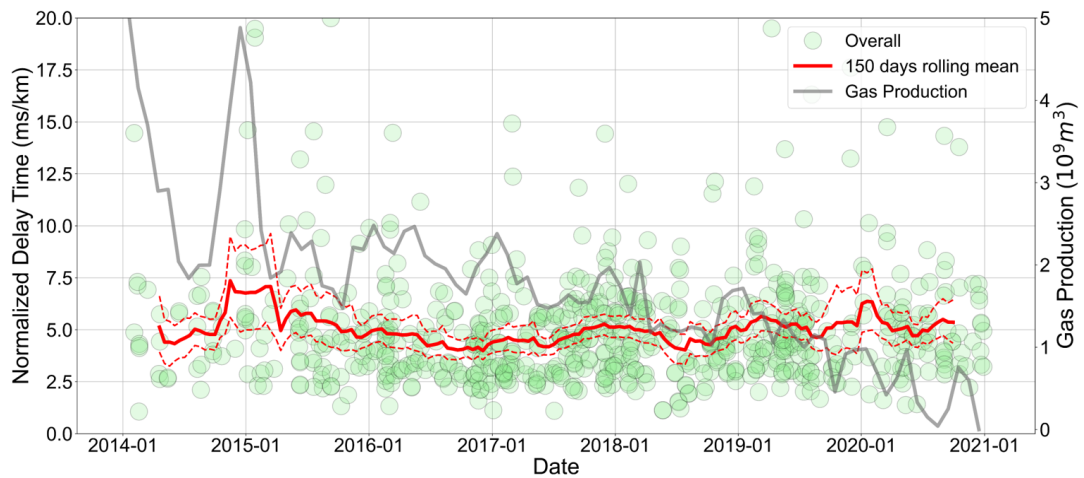


Figure S9. Temporal variation of δtn for the full data catalog. Red solid line shows a 150-day moving mean value with a 15-day step, and red dashed lines for 95% confidence interval. Gray solid line indicates monthly gas production of the Groningen gas field (NAM, 2022).

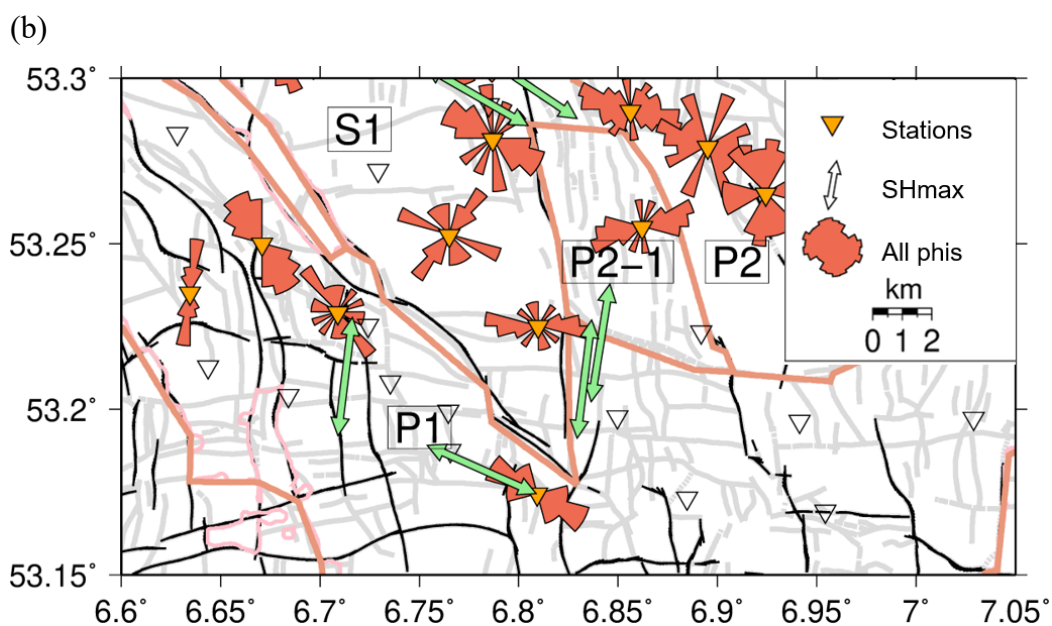
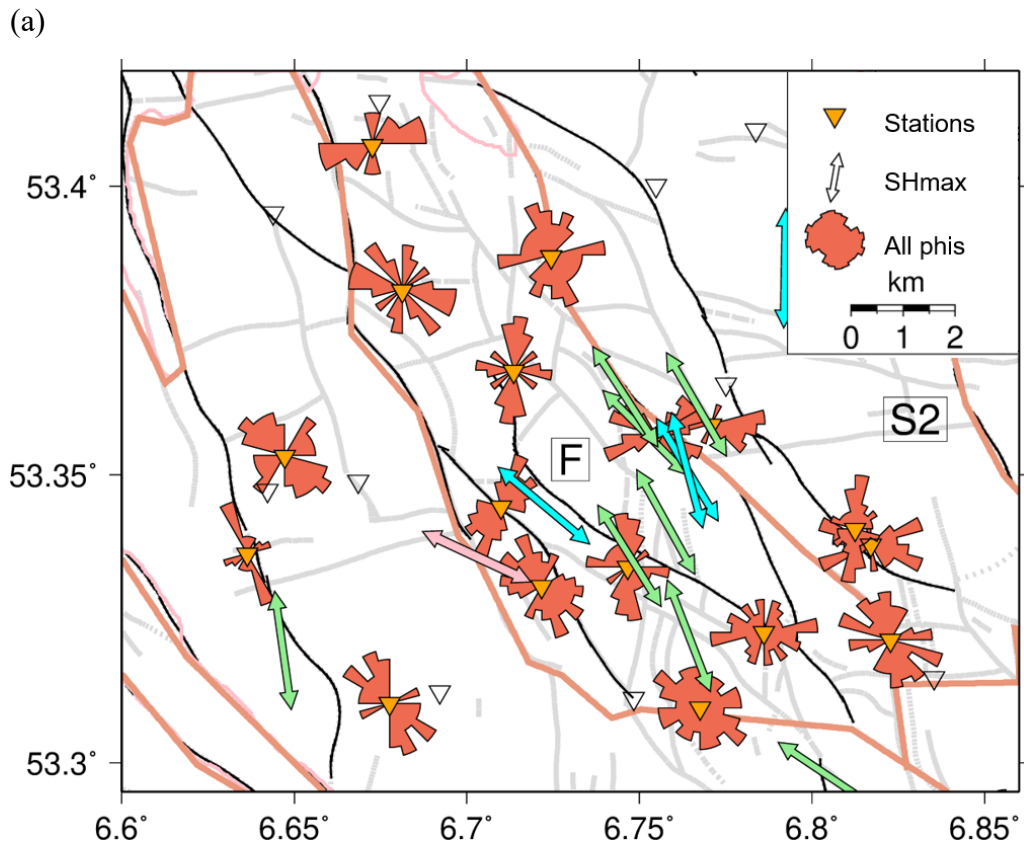


Figure S10. Histogram of φ for stations in Groningen (enlarged from Figure 10a). (a) φ values at northern Groningen. (b) φ values at southern Groningen.

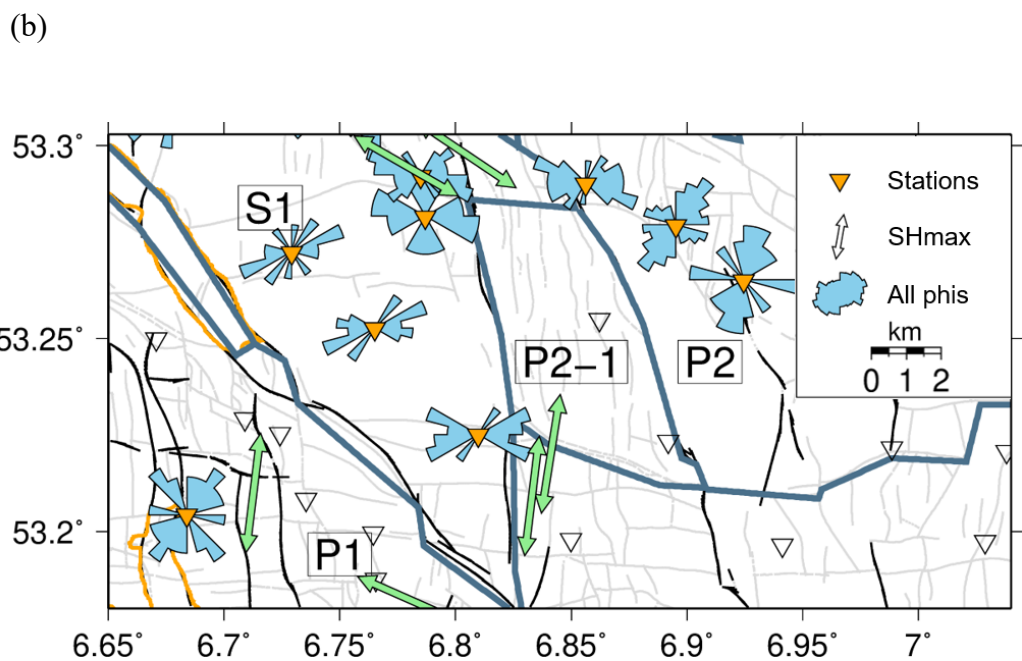
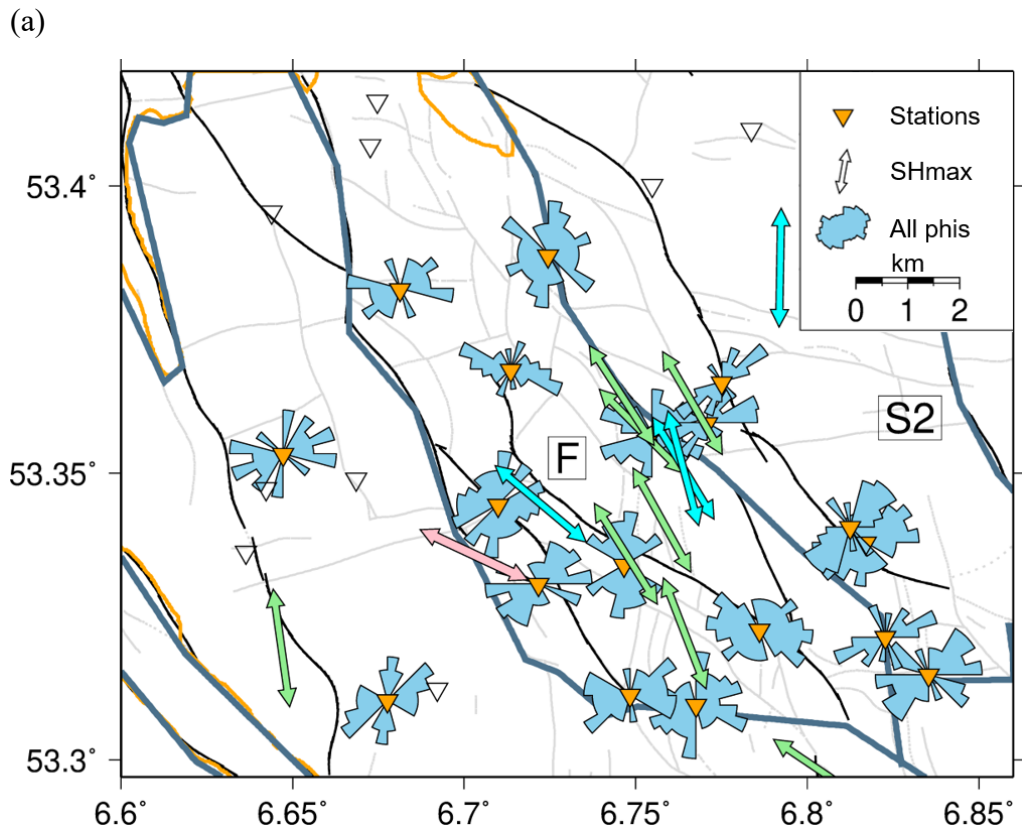


Figure S11. Histogram of null measurements for stations in Groningen (enlarged from Figure 10b). (a) Null values at northern Groningen. (b) Null values at southern Groningen.

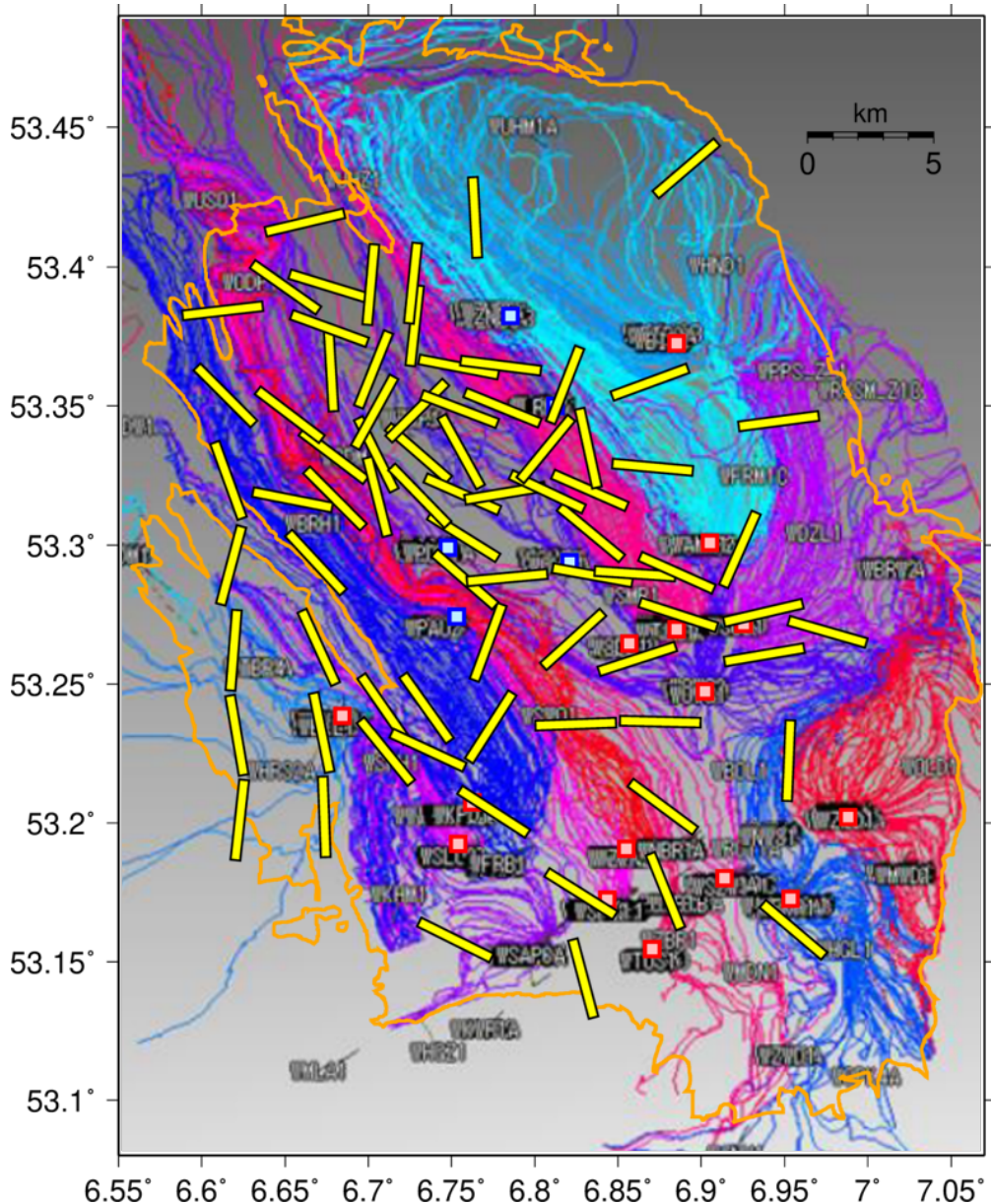


Figure S12. Streamline map (taken from figure 1 in NAM, 2017) overlaid with the spatial averages of φ obtained in this study (Figure 11, yellow bars). Red and blue squares indicate shut-in well cluster and production well cluster, respectively. The map shows expected gas flow at the reservoir, and the streamlines flowing toward different production wells are colored differently.

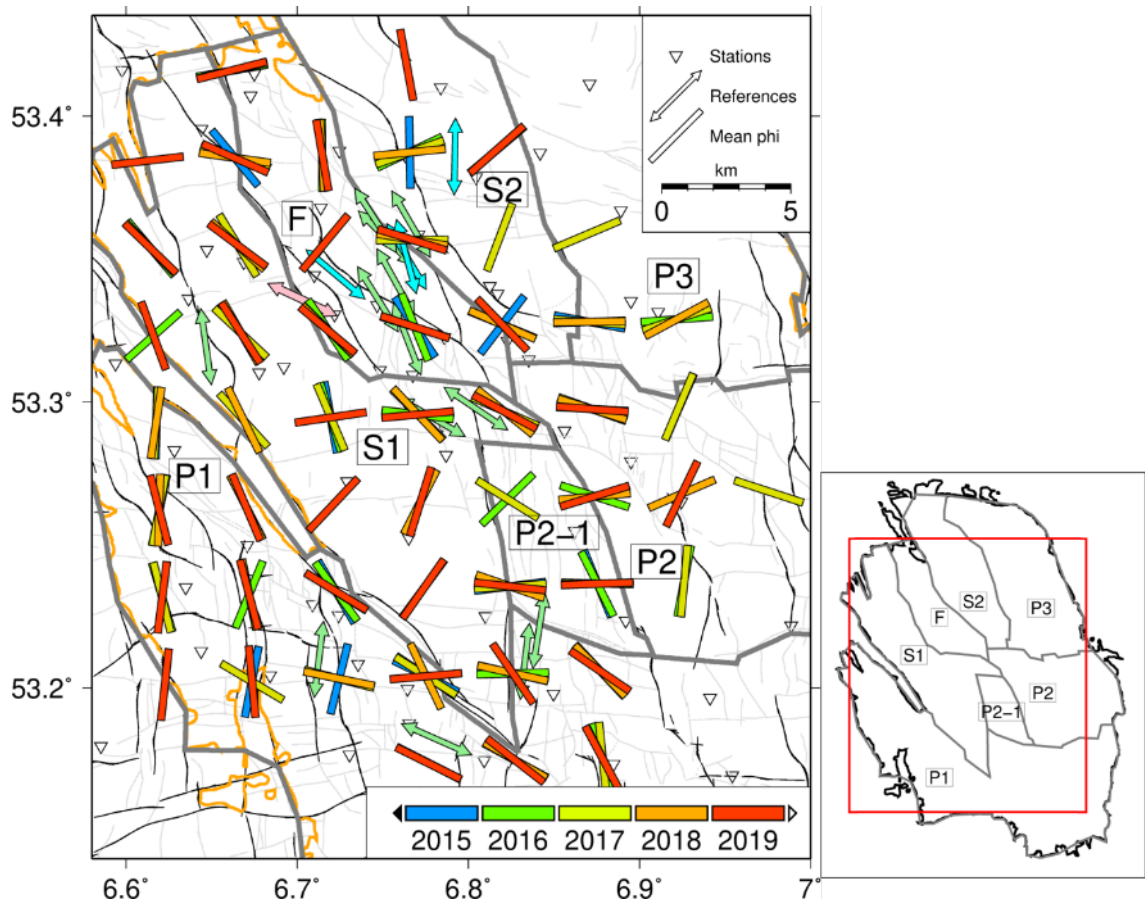


Figure S13. Spatio-temporal distribution of φ in the period of 2014 to 2020. Mean value of φ is color-coded with different periods of the dataset. Double-headed arrows represent maximum horizontal stress directions as the reference (pink: Zhou & Paulissen, 2017, cyan: van Eijs et al., 2015, green: Dost et al., 2020).

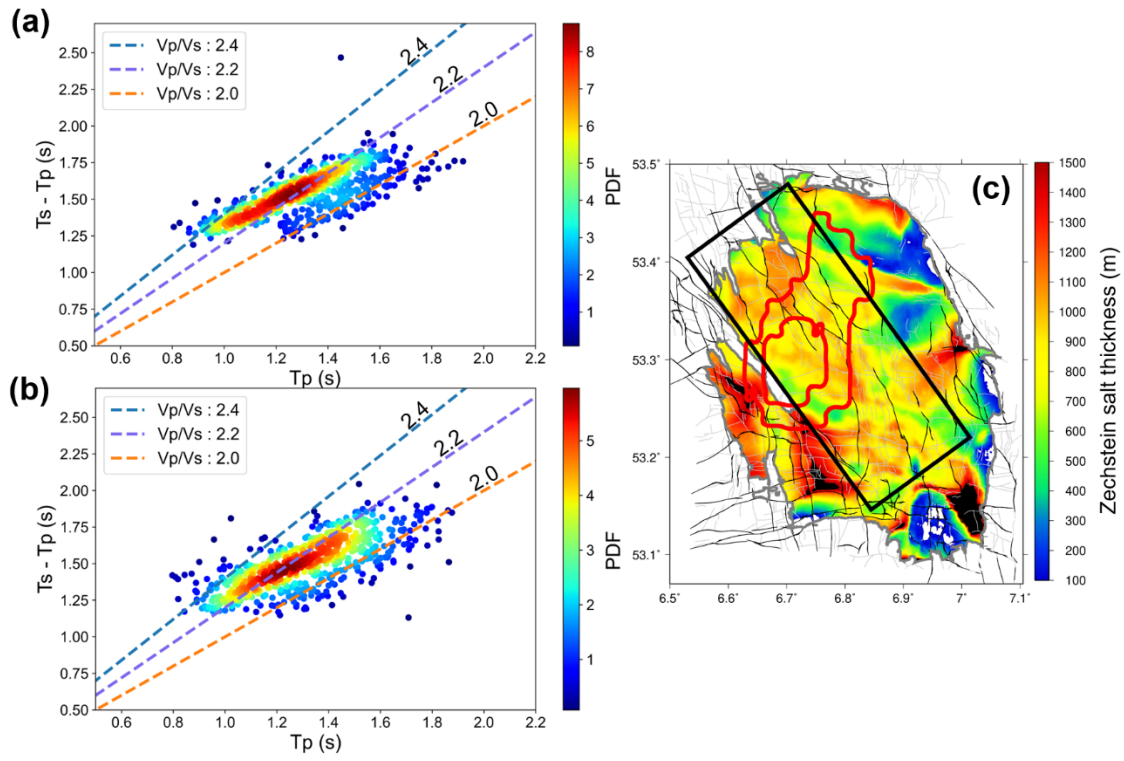


Figure S14. Modified Wadati plot for V_p/V_s ratio. (a) V_p/V_s ratio from the events that occurred in the area showing large compaction of the reservoir (Figure 7a, outer white contour line). (b) V_p/V_s ratio from the events that occurred in the region outside such area. Colors represent probability density functions (PDFs) estimated from the data points. (c) Zechstein salt isopach in Groningen. We only considered the region enclosed in a black box, showing minimal thickness variation, for computing V_p/V_s ratios that are shown in (a) and (b).

References

- Dost, B., van Stiphout, A., Kühn, D., Kortekaas, M., Ruigrok, E., & Heimann, S. (2020). Probabilistic Moment Tensor Inversion for Hydrocarbon-Induced Seismicity in the Groningen Gas Field, the Netherlands, Part 2: Application. *Bulletin of the Seismological Society of America*, 1–12. <https://doi.org/10.1785/0120200076>
- Johnson, J. H., Savage, M. K., & Townend, J. (2011). Distinguishing between stress-induced and structural anisotropy at Mount Ruapehu volcano, New Zealand. *Journal of Geophysical Research: Solid Earth*, 116(12), 1–18. <https://doi.org/10.1029/2011JB008308>
- Nederlandse Aardolie Maatschappij (2017). Groningen Dynamic Model Update 2017. NAM Report. <https://nam-onderzoeksrapporten.data-app.nl/reports/download/groningen/en/d67cb8ac-e5b0-4130-9598-5b7fc83edae2> (last accessed October 2021)
- Nederlandse Aardolie Maatschappij (2022, January 29). Gas-en olie productiecijfers. Retrieved from <https://www.nam.nl/gas-en-olie/gaswinning.html#vanity-aHR0cHM6Ly93d3cubmFtLm5sL2ZlaXRlbi1lbi1jaWpmZXJzL2dhc3dpbm5pbmcuaH>
- Teanby, N. A., Kendall, J. M., & van der Baan, M. (2004). Automation of shear-wave splitting measurements using cluster analysis. *Bulletin of the Seismological Society of America*, 94(2), 453–463. <https://doi.org/10.1785/0120030123>
- van Eijs, R. M. H. E. (2015). Neotectonic Stresses in the Permian Slochteren Formation of the Groningen Field. NAM Report (EP201510210531).

Zhou, W., & Paulssen, H. (2017). P and S Velocity Structure in the Groningen Gas Reservoir

From Noise Interferometry. *Geophysical Research Letters*, 44(23), 11,785-11,791.

<https://doi.org/10.1002/2017GL075592>